Computational and Structural Biotechnology Journal 21 (2023) 5515–5522

Contents lists available at ScienceDirect

Computational and Structural Biotechnology Journal

journal homepage: www.elsevier.com/locate/csbj

Research article

Binding asymmetry and conformational studies of the AtGSDA dimer

Qian Jia [a], Hui Zeng [a], Mingwei Li [b], Jing Tang [a], Nan Xiao [a], Shangfang Gao [a], Huanxi Li [a], Jinbing Zhang [a], Zhiyong Zhang [c,*], Wei Xie [a,*]

[a] MOE Key Laboratory of Gene Function and Regulation, State Key Laboratory for Biocontrol, School of Life Sciences, Sun Yat-Sen University, Guangzhou, Guangdong 510006, People's Republic of China

[b] Division of Life Sciences and Medicine, and Biomedical Sciences and Health Laboratory of Anhui Province, University of Science and Technology of China, Hefei, Anhui 230026, PR China

[c] MOE Key Laboratory for Membraneless Organelles & Cellular Dynamics, Department of Physics, University of Science and Technology of China, Hefei, Anhui 230026, PR China

ARTICLE INFO

Keywords:
Binding asymmetry
Guanosine deaminase
Molecular dynamics simulation
Purine metabolism
Unequal conformation

ABSTRACT

Guanosine deaminase (GSDA) is an important deaminase that converts guanosine to xanthosine, a key intermediate in nitrogen recycling in plants. We previously solved complex structures of *Arabidopsis thaliana* GSDA bound by various ligands and examined its catalytic mechanism. Here, we report cocrystal structures of AtGSDA bound by inactive guanosine derivatives, which bind relatively weakly to the enzyme and mostly have poor binding geometries. The two protomers display unequal binding performances, and molecular dynamics simulation identified diverse conformations during the enzyme-ligand interactions. Moreover, intersubunit, tripartite salt bridges show conformational differences between the two protomers, possibly acting as "gating" systems for substrate binding and product release. Our structural and biochemical studies provide a comprehensive understanding of the enzymatic behavior of this intriguing enzyme.

1. Introduction

Guanine-based purines (GBPs) are endogenous cellular molecules containing the guanine (G) moiety, which include the guanosine nucleotides (GTP/GDP/GMP, etc.), the guanosine nucleoside and the guanine nucleobase [1]. The fates of GBPs are very similar to those of their close relative adenine-based purines (ABPs) [2,3]. They are released by many cell types and interconverted by several enzymatic steps: guanosine (Gua) is initially converted to guanine by purine nucleoside phosphorylase, followed by deamination to xanthine by guanine deaminase (GDA) [4–6]. Complete catabolism ultimately produces uric acid. Due to their participation in important biological processes, including the purine salvage pathway, GBPs and relevant enzymes have been implicated in various diseases. For example, the roles of GBPs as neuromodulators have been well characterized [7]. Under oxidative stress, excessive xanthine appears to promote DNA damage [8]. Moreover, there is a correlation between GBPs and cancers due to their roles in maintaining nucleotide pools. Gua, G and guanosine monophosphate (GMP) have been shown to exert anti-proliferative effects in glioblastoma cells, prostate cancer cells, lung adenocarcinoma cells and myeloid leukemia cells [7,9,10].

The GDA enzyme (EC: 3.5.4.3) catalyzes the hydrolysis of substrates bearing amide, halogen, ester and other functional groups. Many of these substrates are catabolites of purines and pyrimidines. GDA belongs to two superfamilies: the amidohydrolase (AHS) and cytidine-deaminase like (CDA) superfamilies. GDAs from most eukaryotes belong to the AHS superfamily and display the typical $(\beta/\alpha)_8$-barrel fold, while bacterial GDAs have the αβα sandwich fold unique to the CDA superfamily [6]. The first GDA structure was from *Bacillus subtilis* and was reported in 2004 (PDB 1WKQ) [11]. GDAs are distinguished by the conserved motifs of H(C)XE and PCXXC and employ a dual proton shuttle mechanism with two critical glutamates for zinc-dependent deamination. In 2013, Bitra

Abbreviations: ABPs, adenine-based purines; Ado, adenosine; AHS, amidohydrolase; AtGSDA, *Arabidopsis thaliana* guanosine deaminase; CADA, cationic dummy atom; CDA, cytidine-deaminase like; cMD, conventional molecular dynamics; FAcD, fluoroacetate dehalogenase; G, guanine; GBPs, guanine-based purines; GDA, guanine deaminase; GMP, guanosine monophosphate; Gua, guanosine; Ins, inosine; isoG, isoguanosine; m^1G, 1-methylguanosine; m^7G, 7-methylguanosine; NA, not applicable; ns, not significant; N^2-mG, N2-methylguanosine; QM/MM, quantum mechanics/molecular mechanics; R, ribose; s.d., standard deviation; TSA, thermal shift assay; TSBs, tripartite salt bridges; WT, wild type; Xan, xanthosine; 2′-O-mG, 2′-O-methylguanosine; 6-O-mG, 6-O-methylguanosine; 7dzG, 7-deazaguanosine.

* Corresponding authors.
E-mail addresses: zzyzhang@ustc.edu.cn (Z. Zhang), xiewei6@mail.sysu.edu.cn (W. Xie).

https://doi.org/10.1016/j.csbj.2023.11.004
Received 18 August 2023; Received in revised form 1 November 2023; Accepted 1 November 2023
Available online 4 November 2023

et al. systematically studied the binding modes and substrate specificity of GDA from *Nitrosomonas europaea* (NE0047) [12]. In addition to the conserved Glu79, NE0047 also contains Glu143, which plays pivotal roles in deamination. Follow-up hybrid quantum mechanics/molecular mechanics (QM/MM) calculations indicated that the first Zn-bound proton transfer to guanine is mediated by Glu79, while the second is mediated by Glu143. Asn66 plays a key role in substrate anchoring and participates in catalysis. The study also revealed the importance of the C-terminal loop (N181-C189) closure and maintenance of the hydrophobic core by capping residues Phe141 and Phe48 (Supplementary Fig. S1) [13,14].

The main product of purine nucleotide catabolism is xanthosine (Xan), not hypoxanthine or inosine (Ins). Dahncke et al. discovered that xanthosine is exclusively generated from guanosine by a guanosine deaminase (GSDA, EC: 3.5.4.15) in *Arabidopsis* [15]. Phylogenetic analyses indicate that GSDA is predominantly found in plants [15,16]. Mutants of *gsda* have been reported to show phenotypes of impaired growth, delayed germination, reduced recovery after dark treatments, yellowing, etc. [17,18]. Previously, we reported crystal structures of GSDA from *Arabidopsis thaliana* (AtGSDA) in apo- and substate/product-bound forms and proposed a catalytic model. During deamination, both the enzyme and the substrate undergo conformational changes. Interestingly, in both complexes, the essential C-terminal loops of the enzyme of both protomers become fully ordered, forming the key Tyr185/OH-N7 hydrogen bond and enclosing the active sites. We refer to this conformational state as “in/in”. We further reported structures of AtGSDA bound by various ligands, including substrates and inhibitors [19,20]. Most of these ligands are bound in a conserved mode exhibited by the genuine substrate (Gua) or the corresponding product (Xan). These cocrystal structures demonstrated that the C-terminal loops between the two different protomers exhibit structural discrepancies, depending upon the nature of the bound ligands (Supplementary Fig. S2). These findings suggested that the C-termini are subjected to constant conformational changes, and the structural differences are functionally important.

In this study, we determined AtGSDA structures complexed with other ligands (1-methylguanosine, 7-methylguanosine, 6-O-methylguanosine, and 7-deazaguanosine) and revealed new binding features of AtGSDA. Specifically, the two protomers of the dimeric enzyme exhibit binding asymmetry and may adopt the unequal “in/out” conformation combination in the presence of specific ligands. That is, the C-terminus of one chain contacts the solvent instead of the ligand. Last, we found that the structural rearrangements appear to be regulated by a cross-subunit ligand gating system.

2. Materials and methods

2.1. Cloning, expression and protein purification

The expression and protein purification protocols were described previously [19]. The gene encoding AtGSDA (*At5g28050*, accession number NM_122688.4) was cloned from the cDNA of *Arabidopsis thaliana* (Col-0) using restriction sites for *Nde*I and *Xho*I, digested, and ligated into a pET-21b (+) vector. For crystallization, the Ser29-Tyr185 fragment (the SF form) was subcloned and inserted into an engineered pET-28a (+) vector (MerckMillipore). The cloned gene fragment was sequenced to verify the fidelity of the PCR amplification. All mutations were generated using the QuikChange method (Stratagene). The vector was overexpressed in BL21(DE3) cells (Novagen) and purified by affinity chromatography using a HisTrap column and anion-exchange chromatography Hitrap Q HP column (GE Healthcare). Additional information is as previously reported [19].

2.2. Crystallization and structure determination

For the cocrystallization of the complexes, AtGSDA-SF variants were mixed with ligands at different molar ratios, and finally obtained better quality crystals at diffenet molar ratios, with the final concentration of the protein at 8.0 mg/mL. It was found that the ratio of 1:10 gave the best crystals. All of the cocrystals were obtained in a condition of 1.5 M Na-citrate and 0.1 M HEPES (pH 7.5) at 4 ℃. Crystals typically appeared after 1 week, and reached the maximum size after 2 weeks. Crystals were cryoprotected by a brief washing (~10 s) in a reservoir solution supplemented with 10% glycerol. Then they were immediately flash-cooled in liquid nitrogen. Data were collected at − 173.1 °C on a CMOS hybrid pixel detector (Pilatus3 6 M) at the Beamline 19U1 (BL19U1) of the Shanghai Synchrotron Radiation Facility (SSRF, Shanghai, P.R. China) [21]. The data reduction step was performed by the *HKL3000* package [22]. The structures were solved using the molecular replacement (MR) method, phased with the structure of apo-GSDA (PDB 7DBF) as the search model. The structure refinement and manual model building were carried our using the program Phenix and Coot [23,24], respectively. The final model was validated by SFCHECK [25]. All the data collection and structure refinement statistics were summarized in Supplementary Table S1. The structural figures were produced with PyMOL (www.pymol.org).

2.3. Thermal shift analysis

A 20-μl assay mixture containing 1.0 mg/mL GSDA (the full-length form), 1 × SYPRO orange fluorescence dye (Sigma-Aldrich) and 2 mM ligand was mixed in 96-well PCR plates. The Tm is measured using a real-time PCR system (Life Technologies) and the parameters used in the thermal cycler program were described previously [19]. The fluorescence signals of the dye at 490/530 nm wavelengths (for excitation and emission, respectively) during the thermal denaturation were recorded every 30 s. The melting curves of the mutants were fitted by a Boltzmann model with Origin 8.0 software (OriginLab) to derive the melting temperature. The assays were conducted in triplicates for all the mutants and the control samples.

2.4. Simulated systems and conventional molecular dynamics (cMD) simulations

Crystal structures for simulated systems include apo-WT, WT-Xan, WT-m^{7}G, WT-Ins, WT-7dzG, Y185F-Gua, and E82Q-Gua complexes (PDBs 7DBF, 7DCA, 7DOX, 7DCB, 7DOW, 7DQN and 7DC9). cMD simulations were carried out for apo-WT, WT-Xan, WT-m^{7}G, WT-Ins, WT-7dzG, Y185F-Gua, E82Q-Gua, Y185F-Gua2 and WT_Cout by the Amber20 package [26]. Each system was built in the tleap module using the ff19SB force field for protein [27,28]. The parameters of ligands were obtained by GAFF [29]. Zinc ions were modeled by the cationic dummy atom (CADA) method [30]. The structures were immersed into a truncated octahedral box that extended 10 Å away from the solute border, using the OPC water model and periodic boundary conditions [31,32]. More computational details including box dimension, water molecules, number of ions and total atoms were list in Supplementary Table S2. The water molecules and ions were initially minimized for 2000 steps using the steepest descent method for the first 1000 steps and then the conjugate gradient algorithm for the last 1000 steps, with the position of protein and ligands fixed (force constant was 500 kcal mol^{-1} Å^{-2}). In the second energy minimization stage, the restraints on the protein and ligands were removed. This stage was conducted for 2500 steps, using the steepest descent method in the first 1000 steps and then the conjugate gradient algorithm for the last 1500 steps. After that, a heat-up MD was run at a constant volume. The system was heated from 0 to 300 K for 100 ps with a weak restraint of 10 kcal mol^{-1} Å^{-2} on the solute. Then, free MD simulations were carried out under the 300 K in isothermal-isobaric (NPT) condition. The temperature was regulated using the Langevin dynamics with a collision frequency of 1.0 ps^{-1} [33,34]. Pressure was controlled with isotropic position scaling at 1 bar with a relaxation time of 2.0 ps. All of the bonds involving hydrogen atoms

were constrained using the SHAKE algorithm [35]. A 2-fs integration step was used. The long-range electrostatic interactions were calculated using PME method with a 10 Å cutoff for the range-limited non-bonded interactions [36]. 1 μs cMD simulation was performed for each system. The MD simulations were performed utilizing the GPU accelerated pmemd.cuda code under 4352 CUDA cores (NVIDIA GeForce RTX 2080 Ti). The operating systems is linux version 3.10.0–1160.el7.x86_64 (Red Hat 4.8.5–44). The value of RAM available to the working station is 376 G.

3. Results

3.1. Inhibitors that loosely bind to AtGSDA

AtGSDA displays high specificity toward a limited number of substrates, including guanosine, 2′-O-methylguanosine (2′-O-mG) and N2-methylguanosine (N^2-mG) [20]. To explain the enzyme's narrow selectivity, we previously crystallized AtGSDA bound by various ligands, including substrates and inhibitors, in conserved modes, as we observed in the initial binding or postreaction complexes [19,20]. Most ligands were bound with high occupancies and displayed well-defined densities. Additionally, the enzyme made extensive contacts with the base and sugar rings. The structures of the two protomers of the dimeric enzyme, along with their bound ligands, were symmetrical, and were structurally and functionally equivalent. We discovered that guanosine derivatives such as inosine (Ins), adenosine (Ado), and isoguanosine (isoG) failed to activate AtGSDA due to their lack of a 2-amino group [20]. However, it remained difficult to explain why methylated guanosines such as 6-O-methylguanosine (6-O-mG) cannot be converted by AtGSDA. Additionally, on a few occasions, one of the protomers displayed an alternative conformation at its C-terminus or their bound ligands showed relatively large differences in temperature factors compared to their counterparts from the other protomer (PDBs 7DCB, 7W1Q and 7DQN). Notably, the Y185F-Gua complex contained only a singly bound ligand molecule, implying that the other ligand molecule had been released or was yet to be bound (PDB 7DQN). To further investigate the binding modes of AtGSDA, we solved additional AtGSDA structures complexed with several more ligands: 6-O-mG, 1-methylguanosine (m^1G), 7-methylguanosine (m^7G), and 7-deazaguanosine (7dzG). These ligands typically possess extra methyl groups at various positions on the purine ring, among which m^1G and m^7G allegedly play epigenetic roles [37–40]. These cocrystal structures revealed additional important binding features of AtGSDA, as described below.

6-O-mG is well covered by electron density (the chemical structure of the ligand is shown on the side, PDB 7DOY, Fig. 1A and Supplementary Fig. S3). The attachment of the extra methyl group disrupts the original hydrogen bond between O6 and the main chain nitrogen of Ala81, thus nudging the ligand out of the optimal binding site and reducing its binding capability. Compared to the genuine substrate guanosine bound by E82Q (PDB 7DC9, Fig. 1B and Supplementary Fig. S3), the ligand purine ring (indicated by the red arrow) rotates slightly, which probably accounts for the undefined density of the methyl group as well as its inconvertibility to the product (Fig. 1C and Supplementary Fig. S3). The key hydrogen bond between Tyr185 and N7 and the catalytic water remains, but the latter shifts slightly in position. On the other hand, Asn69 no longer forms a hydrogen bond with O6.

m^7G carries a positive charge at N7 of guanosine due to the presence of an extra methyl group, which is delocalized across the purine ring, and the N7 atom without the methyl group originally forms the key hydrogen bond with Tyr185 to seal the active site (PDB 7DOX, Fig. 1D and Supplementary Fig. S3). The methyl group of m^7G breaks this hydrogen bond, increasing the distance between the N7 and OH atoms from the 2.99 Å observed in the E82Q-Gua complex structure (PDB 7DC9) to 3.65 Å [19]. The contact between the nucleoside and Asn69 is also lost. Similar to m^7G, m^1G also carries a positive charge. Because the substrate-binding pocket is relatively hydrophobic and primarily

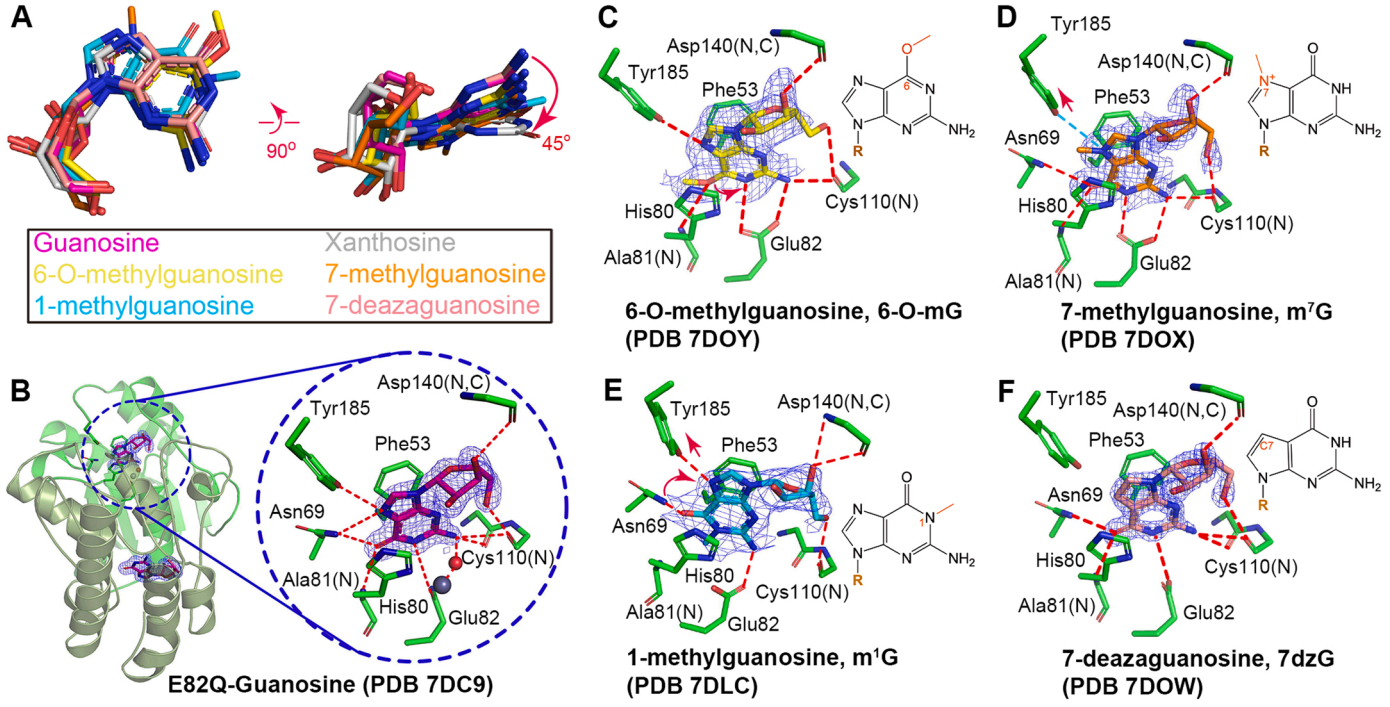

Fig. 1. The binding modes of various ligands. (A) The superimposition of different ligands after reactions with the WT enzyme or E82Q. The coloring scheme is shown in the inset. (B-F) Omit electron density maps showing the interactions of the ligands guanosine (bound by E82Q (B)), 6-O-methylguanosine (C), 7-methylguanosine (D), 1-methylguanosine (E), and 7-deazaguanosine (F) with the enzyme. The hydrogen bonds are indicated by the red dashed lines. PDBs: 7DC9, 7DOY, 7DOX, 7DLC and 7DOW. The maps are contoured at 2σ, and only the more tightly bound ligands (with more defined density) in the dimeric enzyme are shown. The chemical structures of the ligands are drawn, with their unique parts colored in red. R: ribose. The red arrows in Figs. 1D and 1E indicate the movement of the residue (moving far away), whereas the cyan line in Fig. 1D indicates the loss of the hydrogen bond between Tyr185 and N7.

composed of aromatic residues, including Phe53, Phe139, Phe142, Leu119, and Tyr185 (PDB 7DLC, Fig. 1E and Supplementary Fig. S3), the charged substrates are not expected to bind as strongly as the genuine substrate. This is further supported by the poorer electron density covering this ligand. The superposition of the two protomers showed that the C-termini of the two protomers, as well as their ligands (m^1G or m^7G), did not align well, implying that the ligands were bound in different poses at their active sites.

7dzG is interesting due to the absence of N7. In the cocrystal structure with 7dzG, the binding orientation and angle are nearly identical to those of guanosine (Fig. 1A). Interestingly, the C-terminus of one chain does not loop back but points to the solvent instead (referred to herein as the "out" conformation), reminding us of the minor conformation observed in the WT-Ins or Y185F-Gua complexes (PDBs 7DCB and 7DQN) [20]. The absence of N7 in this ligand inhibitor results in the simultaneous loss of two key hydrogen bonds with Tyr185 and Asn69 (PDB 7DOW, Fig. 1F and Supplementary Fig. S3). 7dzG is inert to AtGSDA, even though it is bound by both protomers in perfect geometries. The loss of two key interactions may contribute to the release of the C-tail and the opening of the active site in one of the protomers, which explains the inactivity of AtGSDA. Nevertheless, this protomer still binds a 7dzG molecule, even though it shows weaker density than that bound by the other protomer. This result also suggests that both active sites need to be sequestered (i.e., the "in" conformation) for the enzyme to be reasonably active.

In summary, these methylated forms of guanosine bind in a similar but nonoptimal mode at the active sites of the enzyme. This is consistent with their generally poorer density in one of the protomers compared to the other (in Fig. 1, only the ligand with the better density is shown). Moreover, the catalytic water molecules are retained, although they may move slightly away from their original positions due to the structural perturbation caused by the bound ligands. Although we observed small-angle rotations (20–30 degrees) of the purine rings in some ligands compared to that of guanosine in complex with E82Q (Fig. 1A), the densities of these ligands were not well defined. Please note that these cocrystal structures only show averaged results of multiple deamination reactions and may not accurately represent the individual states of each enzyme molecule. Additionally, we failed to detect their corresponding products through kinetic studies or mass spectrometry (data not shown), indicating their nonreactivity.

We previously investigated the binding affinities of the enzyme toward the substrates and inhibitor compounds using a thermal shift assay (TSA) [20]. To understand the specific catalytic efficiency of AtGSDA toward different compounds, we measured the binding affinities of the enzyme toward the abovementioned methylated guanosine derivatives. As shown in Fig. 2A, all of these molecules enhanced the stabilities of the resulting enzyme-compound complexes, as evidenced by increases in their Tm values compared to the apo-form (Fig. 2B). Most compounds showed reasonable binding behaviors, with Gua, Xan and 2′-O-mG generating the largest shifts of ~1.5 ℃ or above in Tm values, while the compounds N^2-mG, Ado and isoG had the smallest shifts [20]. The commonality among these three compounds is that their respective substituents affect the original hydrogen bond with N2 of guanosine. From TSA, we also learned that G would not be converted to its deaminated form due to its poor binding to the enzyme (no shift), which suggested that the interactions on the ribose ring are also important for catalysis (Fig. 2B) [20].

3.2. Molecular dynamics (MD) simulation studies

To further explore the enzyme dynamics, 1-μs MD simulations were conducted on seven representative structures (Supplementary Movie S1). Here, we selected a few representative crystal structures for study: apo-WT, WT-Xan (xanthosine), WT-Ins (inosine), WT-m^7G (7-methylguanosine), WT-7dzG (7-deazaguanosine), E82Q-Gua (guanosine), and Y185F-Gua (guanosine) complexes (PDBs 7DBF, 7DCA, 7DCB, 7DOX,

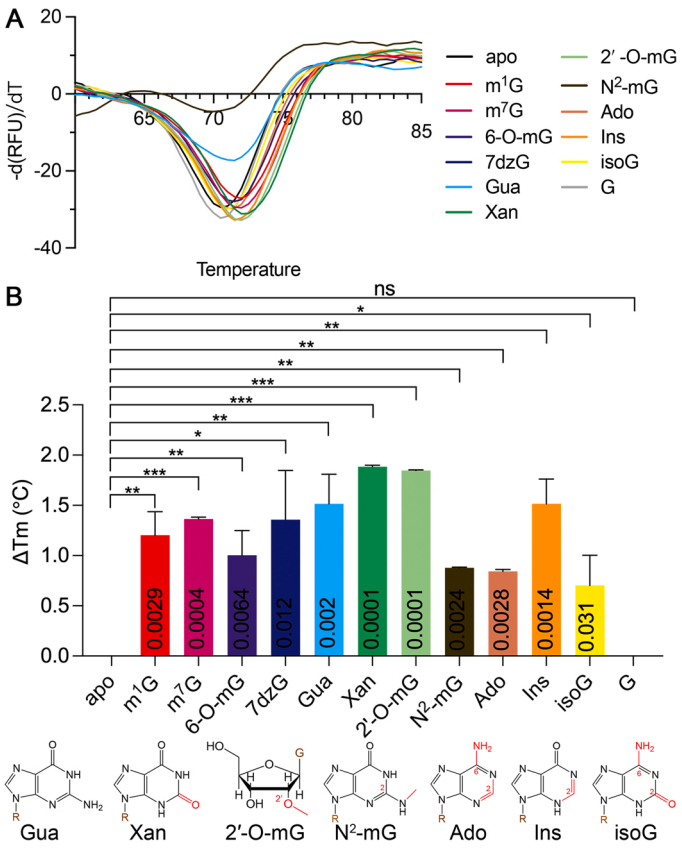

Fig. 2. The thermal shift analysis melting curves of various ligands to AtGSDA. (A) The melting curves of the enzyme in complex with various ligands. The horizontal axis indicates temperature, while the vertical axis indicates fluorescence emission with respect to temperatures (-d(RFU)/dT). (B) Comparison of the stabilizing effects of the ligands. ΔTm represents the changes in Tm values between the complexes and the WT apo-enzyme. Error bars are standard deviation (s.d.) (n = 3 biological replicates). Statistical evaluation with two-way ANOVA was followed by the two-tailed unpaired Student's test. Probability values for pairwise comparisons to apo are shown at the respective bars. * : $p < 0.05$, * *: $p < 0.01$, * ** : $p < 0.001$, ns: not significant. The chemical structures of the ligands are drawn with their unique parts shown in red. m^1G: 1-methylguanosine; m^7G: 7-methylguanosine; 6-O-mG: 6-O-methylguanosine; 7dzG: 7-deazaguanosine; Gua: guanosine; Xan: xanthosine; 2′-O-mG: 2′-O-methylguanosine; N^2-mG: N2-methylguanosine; Ado: adenosine; Ins: inosine; isoG: isoguanosine; G: guanine; R: ribose.

7DOW, 7DQN and 7DC9, respectively). The selection rationale is as follows: the WT-Xan, Y185F-Gua and E82Q-Gua systems are the three systems in which the ligands are the natural product or substrate, respectively. However, the latter two involve partially and completely inactive enzymes [19,20]. On the other hand, the WT-Ins complex represents a system with an alternative conformation of the enzyme, whereas the WT-m^7G and WT-7dzG systems employed ligands that bind with poor geometries (see methods for details). During the simulation, we maintained the stability of Zn^{2+} by applying the cationic dummy atom (CADA) model, which stabilizes the interactions between Zn^{2+} and its coordinating ligands, ensuring that it remains fixed in position. The RMSF curves for the two chains in these structures are fairly similar (Fig. 3A). The tails of both the WT-Xan and E82Q-Gua complexes are located near the active site in their respective structures and behave similarly. However, the average N7-OH distance of the E82Q-Gua complex is larger (~5.3 Å, compared to 3.5 Å for WT) (Fig. 3B, Table 2). Specifically, ~60–70% of conformers from both chains of the WT (out of a total of 1000 during the 1 μs-scale simulation) maintain the important hydrogen bond with Xan if its cutoff distance is set to 3.5 Å, or ~100% of conformers if the cutoff is 4.0 Å, but this relationship is

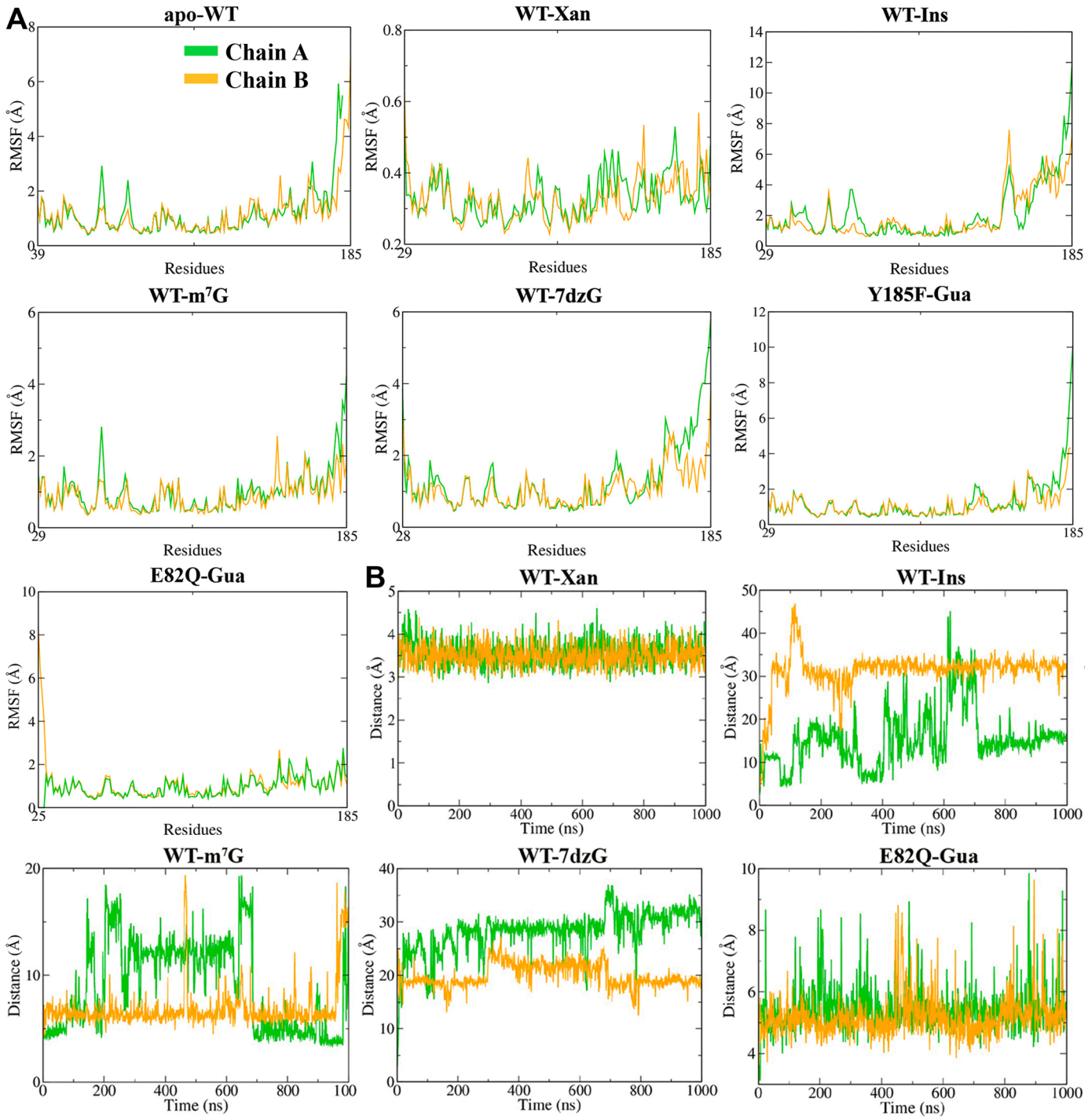

Fig. 3. The protein structural flexibility and ligand perturbability of the representative structures. (A) The MD simulation results of the AtGSDA apo- and ligand-bound structures. The simulation was conducted for 1 μs on seven representative structures, and the evolution of RMSF values (units in Å) for the two chains (colored green and yellow, respectively) is shown. The sequences for the chains normally range from Ser29 to Tyr185, although the resolved residues may vary slightly in different structures. (B) The protein structural flexibility and ligand perturbability of the representative structures. The distance of guanosine/N7-Tyr185/OH during the 1-μs MD simulation. Note that C7 replaces N7 in the 7dzG-WT complex structure, and the Y185F-Gua complex contains only one ligand molecule with the tyrosine residue mutated (thus not monitored). Chains A and B are colored green and yellow, respectively. Xan: xanthosine; Ins: inosine; m^7G: 7-methylguanosine; 7dzG: 7-deazaguanosine; Gua: guanosine.

almost totally disrupted in E82Q (~ only 4% retaining interaction). m^7G binding enhances the conformational imbalance by differentially loosening the C-termini of both chains, and they swing out to the solvent on many occasions. Eleven percent of the conformers in chain A adopt the "in" conformation if the N7-OH distance is restricted to ~3.5 Å, while all B molecules lose this interaction (with distances ranging from ~12.5–17.0 Å, Panel 3). Furthermore, in other structures, even with the "in/in" conformations (7dzG, Ins or E82Q-Gua), one chain constantly switches between the two conformations, while the other chain completely adopts the "out" conformation, as does the apo-enzyme (Supplementary Movie S1). The largest distance between C7 (equivalent to N7)-OH in 7dzG and Tyr185 would exceed 25.0 Å. Additionally,

Table 1
The differential states of the two protomers of AtGSDA bound by various ligands in cocrystal structures.

Cocrystals	Temperature factors (Å^2)		Chain Conformation Combination (A/B)	Space group	Reference
	Protein chains (A, B)	Ligands in A, B			
apo-WT (7DBF)	34.6, 36.5	NA	Disordered/Out	$P6_1$	[21]
WT-Xan (7DCA)	21.4, 19.7	16.5, 15.9	In/In	$P6_1$	[21]
E82Q-Gua (7DC9)	31.0, 31.8	26.6, 30.3	In/In	$P6_1$	[21]
WT-2'-O-mG (7DGC)	37.3, 36.0	42.7, 41.3	In/In	$P6_1$	[20]
WT-N^2-mG (7DH1)	33.7, 31.4	31.1, 31.9	In/In	$P6_1$	[20]
WT-isoG (7DM6)	20.9, 18.5	19.3, 18.3	In/In	$P6_1$	[20]
WT-Ado (7DCW)	23.2, 22.4	19.1, 21.9	In/In	$P6_1$	[20]
WT-Ins (7DCB)	32.5, 35.3	30.0, 38.6	In/In, double conformations for B	$P6_1$	[20]
WT-m^7G (7DOX)	18.1, 18.5	26.1, 27.0	In/In	$P6_1$	This work
WT-6-O-mG (7DOY)	35.4, 35.2	43.0, 46.0	In/In	$P6_1$	This work
WT-m^1G (7DLC)	27.9, 28.7	40.8, 40.3	In/In	$P6_1$	This work
WT-7dzG (7DOW)	27.5, 28.5	22.6, 30.1	In/Out	$P6_1$	This work
Y185F-Gua (7DQN)	30.4, 24.8	31.5 (only one ligand)	In/Out, F185 in chain B invisible	$P6_1$	[20]
E82Q-2′-O-mG (7W1Q)	26.8, 28.9	30.3, 41.4	In/Out	$P6_1$	[20]

Tyr185 barely closes the active sites during the simulation. This exposure of the active sites partially explains the low reactivity of AtGSDA.

Last, we simulated the Y185F-Gua (guanosine) complex, which is unique because only one chain contained the substrate. We wondered how it would behave if it were a balanced dimer. We therefore modeled a second guanosine molecule in the empty chain and looped its C-terminus back into the active site (Y185F-Gua2, Supplementary Movie S1). Both C-termini of the hypothetical dimer remain longer in the active site than in the singly guanosine-bound case, but they eventually break free and return to the solvent. A total of 98% and 64% conformations of the two chains are "out", respectively. Therefore, the "out" conformation suggests that the enzyme waits for its C-terminus to close to start/resume the reaction because the reaction is still incomplete, or the enzyme is preparing to release the ligands because it has trouble converting the ligands into products due to improper closing. Similarly, we made an artificially equivalent full-length apo-enzyme with the "out/out" conformations (i.e., both chains have intact C-termini that contact solvent) to investigate the state of the free enzyme (WT_Cout, Supplementary Movie S1), and we found that the tails stay outside the active sites most of the time. However, we occasionally sampled some conformers even when no ligands were present. This result indicates that the apo-enzyme preferentially adopts the "out" conformation to maximize the degrees of freedom.

4. Discussion

Guanosine deaminase is a plant-specific enzyme that catalyzes the deamination of guanosine. It is a part of purine metabolism and is critical for various physiological processes in cells, but the enzyme's high selectivity and dynamics remain unclear. In the previous structures, we observed that the two protomers of the dimeric enzyme function independently and bind equally well toward their substrates (Gua, 2′-O-mG and N^2-mG) or inhibitors (Ado, Ins and isoG) [19,20]. However, close examination of the cocrystal structures in this study revealed that the two protomers of AtGSDA exhibit different behaviors under several circumstances. Specifically, they appear to be asymmetric in action, with one protomer contributing more to ligand binding than the other, especially when nonoptimal ligands or enzyme mutants are involved (PDBs 7DOY, 7DOX, 7DLC and 7DOW). These structures typically exhibit the following characteristics:

First, the structure of the apo-enzyme is asymmetric in that one protomer displays a disordered C-terminus, while the other forms a loop and makes contacts with the solvent (PDB 7DBF) [19]. That is, in the absence of a ligand, the C-termini of the apo-enzyme are conformationally diverse (its electron density in one chain is averaged out while the other is solvent-accessible). Additionally, the solvent-accessible but ordered C-terminus in the other chain should not be interpreted as an artifact of crystal packing. Rather, it should be regarded as a biologically relevant event because the free tails loop back into the active sites once the genuine substrates bind. The engagement of the ligands compensates for the losses of conformational entropies of both the enzyme and substrate. Y185F is only partially active (its k_{cat}/k_m is only 17.9% of WT [19]), and the Y185F-Gua complex containing a singly bound ligand (PDB 7DQN) provides additional evidence that the unequal binding is not a result of crystal packing.

Second, the C-terminus of one protomer frequently exhibits double or alternative conformations or poorer electron density and may even adopt the "out" conformation (Table 1). This imbalance becomes more pronounced in the presence of loosely bound ligands investigated in this study, such as methylated guanosine. In contrast, the other protomer always displays the "in" conformation. Furthermore, in these loosely bound complexes, one ligand sometimes displays a higher temperature factor than the other, or they do not bind at exactly equivalent sites in their respective binding pockets. Additionally, the temperature factors of both ligands are higher than those of their protein chains (Table 1).

Third, the two protomers undergo reactions differentially, especially in challenging deamination cases (due to enzyme mutations). For example, E82Q complexed with 2′-O-mG (PDB 7W1Q) shows modest to large differences in temperature factors of the ligands and exhibits "in/out" conformations (Table 1) [20]. Although the partially active Y185F reacts with guanosine (PDB 7DQN), we observed that one protomer had already released the ligand, while the other ligand remained bound in the cocrystal structure. In the WT-7dzG case, although each protomer of AtGSDA was bound by a 7dzG molecule, the C-terminus of one chain had been released into the solvent (Supplementary Fig. S4). The structural asymmetry is more evident in the MD simulation.

Last, we observed the asymmetric pattern of a cross-subunit salt bridge immediately above the active sites (Fig. 4A). Namely, two salt bridges are formed between Asp140/Chain A, Arg121/Chain B and Tyr185/Chain A, in which the carboxylate group of the terminal residue Tyr185 is involved. This tripartite salt bridge (named TSB-A) centers around the key residue Arg121, whose orientation is subjected to a "tilting" action, depending on the extent of the deamination reaction. We found that TSB-A always existed, while its counterpart Asp140/B-Arg121/A-Tyr185/B (TSB-B) was usually disrupted due to the orientational differences in the side chains of Asp140 and Arg121 between the two protomers. Additionally, the more stable TSB-A is correlated with the more defined electron density of the ligands in chain A. We found that the lockup of such "gating" systems (or the formation of the TSBs) is typically observed in chains whose tails are directed toward the active sites. This indicates that the active sites are sealed and that the ligands are bound more tightly (resulting in good occupancies, Fig. 4B). In contrast, "in/out" conformations correspond to the unlocking of TSB-B and are mainly associated with poor density of the bound ligands in

Table 2
The flexibilities of the C-terminal tails of the protein chains and their bound ligands.

Systems	Chain	WT-Xan	WT-m^{7}G	WT-Ins	WT-7dzG	E82Q-Gua	Y185F-Gua
Conformer percentages forming the N7-OH interaction	A	58.0% (96.2%)*	11.0%	3.0%	1.0%	4.0%	NA
	B	67.0% (98.5%)*	0	0	0	1.0%	NA

* the percentages using 4.0 Å as the cutoff distance; NA: not applicable.

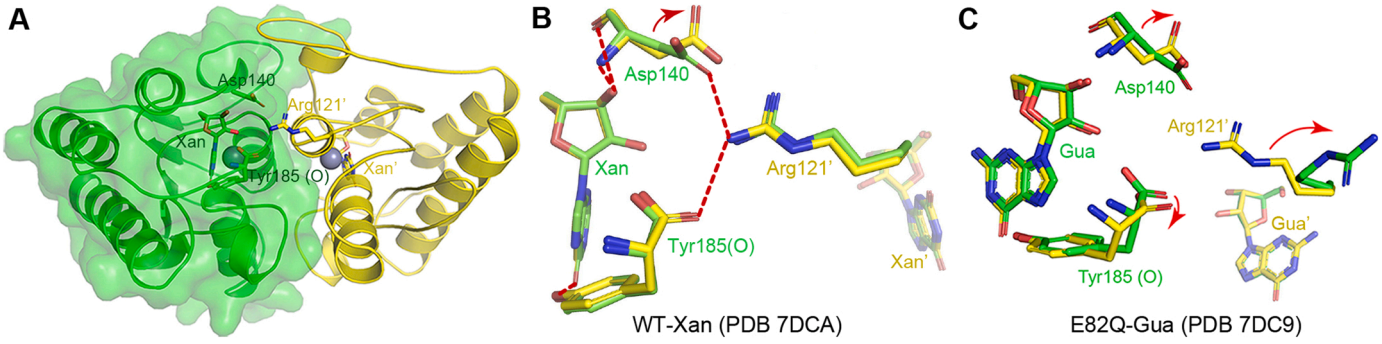

Fig. 4. The importance of TSB and their interaction details. (A) The overall structure and the TSB sites. Chains A and B are colored green and yellow, respectively, and the protomers are shown in surface and ribbon simultaneously. (B) The TSB interaction details in the WT-Xan complexes (PDB 7DCA) and their relationship to Xan, which adopts the "in/in" conformation combination. The TSB-A and TSB-B residues were superimposed. The arrows indicate the positional and orientational differences of the TSB residues between the two chains. (C) The same interactions in the E82Q-Gua complex (PDB 7DC9, "in/out" conformations). Note that the side chain of Arg121 is substantially tilted, which disrupts the original electrostatic interactions. Gua: guanosine; Xan: xanthosine.

chain B. Therefore, we postulate that these TSBs likely act as "gates" and are essential for the release of products/ligands or enzyme regeneration. The backward tilt of Arg121/A disrupts the key contacts with Asp140/B and Tyr185/B, both of which form hydrogen bonds with the ligands during the deamination reaction. This tilting action is more obvious in a nonproductive reaction by a mutant such as E82Q (Fig. 4C).

The above observations suggest the functional importance of the asymmetric binding phenomenon and the role of TSBs in catalysis. A possible explanation is that the conformational changes between the substrate and the product, such as the rotation of the guanine ring after the deamination reaction, may result in alterations in the binding strengths with Asp140 and Tyr185 (both are key residues in substrate/product binding), associated with the release of the product. Indeed, the R121A/Y185F double mutation would reduce the activity to barely 5% of WT (25% for the single mutation R121A) [19]. In contrast, the single mutation Y185F loses the interaction with N7 but retains its free carboxyl group (as it is the very last residue of the C-terminus), and its consequence is not as dramatic as that of either deletion mutation K181 or R183 (the four- or two-residue truncation at the C-termini, respectively), supporting our hypothesis regarding the TSB gating system [19]. Under the regulation of TSBs, both chains bind and release the substrate/product in an orderly manner, consistent with the observations of the differentially bound ligands. These successive steps ensure continuous enzyme turnover.

Currently, we do not have sufficient evidence to determine whether the two protomers would exhibit different catalytic efficiencies. However, asymmetric binding is typically associated with loosely bound ligands or enzyme mutations, suggesting the possibility of such a phenomenon. Furthermore, the activity-impaired mutants E82Q and Y185F also exhibit catalytic asymmetry toward genuine substrates (2′-O-methylguanosine and guanosine, respectively) [19,20]. Since crystal structures are only static snapshots of the enzyme, important kinetic details during catalysis are absent. Hence, we investigated the binding modes and deamination activities of AtGSDA through molecular dynamics simulation, which facilitated the identification and capture of various dynamic flexible conformers, providing a more detailed understanding of the enzyme in action. Although the enzyme binds the ligands similarly to that of the genuine substrate in static crystal structures, MD simulations indicate that the enzyme has difficulty maintaining perfect ligand-binding geometries constantly due to its flexibility at the C-termini and the fluctuations of the ligands at the active sites. Other than the absolute "in" (Tyr185 hydrogen bonds to N7 of guanosine) and "out" conformations (where the last four residues of GSDA extend to the solvent), we also observed numerous nonstandard conformations of the enzyme and poorly aligned ligands at the active centers. The combination of crystallographic and MD simulation studies captured the unequal binding behaviors in enzymatic dynamics. This helped us propose a model in which TSBs play a regulatory role. Further investigations like single-molecule kinetics or complementary MD studies (such as the program MDLovoFit) would reveal more details of AtGSDA catalysis [41].

The homodimeric enzyme fluoroacetate dehalogenase (FAcD) from *Rhodopseudomonas palustris* turns over only one substrate molecule at a time [42,43]. Crystallographic analysis indicates that only one protomer is poised for substrate binding at any instance, and the asymmetry becomes evident upon the binding of the substrate, and conformational exchange increases greatly when the substrate is locked into the binding pocket. The behavior of AtGSDA asymmetry does not follow the "half-of-the-sites" reactivity theory like FAcD because both GSDA protomers can bind and convert the standard substrates equally, a result of the deamination occurring too quickly to be captured by crystallographic studies. Other enzyme examples of asymmetric catalysis include the SARS 3 C-like proteinase and α-catenin [44,45], which will not be further detailed here.

CRediT authorship contribution statement

Qian Jia: Methodology, Validation, Formal analysis, Investigation, Data curation, Writing – original draft, Funding acquisition. **Hui Zeng:** Methodology, Validation. **Mingwei Li:** Methodology, Validation. **Jing Tang:** Methodology, Validation. **Nan Xiao:** Methodology, Validation. **Shangfang Gao:** Methodology, Validation. **Huanxi Li:** Methodology, Validation. **Jinbing Zhang:** Methodology, Validation. **Zhiyong Zhang:** Conceptualization, Investigation and review. **Wei Xie:** Supervision, Conceptualization, Investigation, Writing – original draft, Writing – review & editing, Visualization, Funding acquisition.

Declaration of Competing Interest

The authors declare that they have no known competing financial interests or personal relationships that could have appeared to influence the work reported in this paper.

Acknowledgements

We express thanks to BL19U1 beamlines (National Center for Protein Sciences Shanghai (NCPSS) at Shanghai Synchrotron Radiation Facility, for assistance during data collection. The Supercomputing Center of USTC provides computer resources for this project, and we are grateful to Mr. Yundong Zhang for his technical supports. This work was supported by the National Natural Science Foundation of China [31870782], [32271322] and [91953101], and the Natural Science Foundation of Guangdong Province [2020A1515010965] and [2021A1515010880].

Accession number

Atomic coordinates and structure factors for the reported crystal structures have been deposited with the Protein Data Bank under accession numbers 7DLC, 7DOY, 7DOX and 7DOW.

Appendix A. Supporting information

Supplementary data associated with this article can be found in the online version at doi:10.1016/j.csbj.2023.11.004.

References

[1] Schmidt AP, Lara DR, Souza DO. Proposal of a guanine-based purinergic system in the mammalian central nervous system. Pharm Ther 2007;116(3):401–16.
[2] Santos TG, Souza DO, Tasca CI. GTP uptake into rat brain synaptic vesicles. Brain Res 2006;1070(1):71–6.
[3] Zimmermann H, Braun N. Extracellular metabolism of nucleotides in the nervous system. J Auton Pharm 1996;16(6):397–400.
[4] Yuan G, Bin JC, McKay DJ, Snyder FF. Cloning and characterization of human guanine deaminase. Purification and partial amino acid sequence of the mouse protein. J Biol Chem 1999;274(12):8175–80.
[5] Giuliani P, Zuccarini M, Buccella S, Rossini M, D'Alimonte I, Ciccarelli R, Marzo M, Marzo A, Di Iorio P, Caciagli F. Development of a new HPLC method using fluorescence detection without derivatization for determining purine nucleoside phosphorylase activity in human plasma. J Chromatogr B Anal Technol Biomed Life Sci 2016;1009–1010:114–21.
[6] Shek R, Hilaire T, Sim J, French JB. Structural determinants for substrate selectivity in guanine deaminase enzymes of the amidohydrolase superfamily. Biochemistry 2019;58(30):3280–92.
[7] Oliveira KA, Dal-Cim TA, Lopes FG, Nedel CB, Tasca CI. Guanosine promotes cytotoxicity via adenosine receptors and induces apoptosis in temozolomide-treated A172 glioma cells. Purinergic Signal 2017;13(3):305–18.
[8] Birder LA, Wolf-Johnston A, Wein AJ, Cheng F, Grove-Sullivan M, Kanai AJ, Watson AM, Stoltz D, Watkins SC, Robertson AM, et al. Purine nucleoside phosphorylase inhibition ameliorates age-associated lower urinary tract dysfunctions. JCI Insight 2020;5:20.
[9] Garozzo R, Sortino MA, Vancheri C, Condorelli DF. Antiproliferative effects induced by guanine-based purines require hypoxanthine-guanine phosphoribosyltransferase activity. Biol Chem 2010;391(9):1079–89.
[10] Zhang N, Bing T, Liu X, Qi C, Shen L, Wang L, Shangguan D. Cytotoxicity of guanine-based degradation products contributes to the antiproliferative activity of guanine-rich oligonucleotides. Chem Sci 2015;6(7):3831–8.
[11] Liaw SH, Chang YJ, Lai CT, Chang HC, Chang GG. Crystal structure of *Bacillus subtilis* guanine deaminase: the first domain-swapped structure in the cytidine deaminase superfamily. J Biol Chem 2004;279(34):35479–85.
[12] Bitra A, Hussain B, Tanwar AS, Anand R. Identification of function and mechanistic insights of guanine deaminase from *Nitrosomonas europaea*: role of the C-terminal loop in catalysis. Biochemistry 2013;52(20):3512–22.
[13] Singh J, Gaded V, Bitra A, Anand R. Structure guided mutagenesis reveals the substrate determinants of guanine deaminase. J Struct Biol 2021;213(3):107747.
[14] Sen A, Gaded V, Jayapal P, Rajaraman G, Anand R. Insights into the Dual Shuttle Catalytic mechanism of guanine deaminase. J Phys Chem B 2021;125(31):8814–26.
[15] Dahncke K, Witte CP. Plant purine nucleoside catabolism employs a guanosine deaminase required for the generation of xanthosine in *Arabidopsis*. Plant Cell 2013;25(10):4101–9.
[16] Nygaard P, Bested SM, Andersen KAK, Saxild HH. Bacillus subtilis guanine deaminase is encoded by the yknA gene and is induced during growth with purines as the nitrogen source. Microbiol (Read) 2000;146(Pt 12):3061–9.
[17] Baccolini C, Witte CP. AMP and GMP catabolism in *Arabidopsis* converge on Xanthosine, which is degraded by a nucleoside hydrolase heterocomplex. Plant Cell 2019;31(3):734–51.
[18] Schroeder RY, Zhu A, Eubel H, Dahncke K, Witte CP. The ribokinases of *Arabidopsis thaliana* and *Saccharomyces cerevisiae* are required for ribose recycling from nucleotide catabolism, which in plants is not essential to survive prolonged dark stress. N Phytol 2018;217(1):233–44.
[19] Jia Q, Zeng H, Li H, Xiao N, Tang J, Gao S, Zhang J, Xie W. The C-terminal loop of *Arabidopsis thaliana* guanosine deaminase is essential to catalysis. Chem Commun 2021;57(76):9748–51.
[20] Jia Q, Zhang J, Zeng H, Tang J, Xiao N, Gao S, Li H, Xie W. Substrate specificity of GSDA revealed by cocrystal structures and binding studies. Int J Mol Sci 2022;23:23.
[21] Zhang W, Tang J, Wang S, Wang Z, Qin W, He J. The protein complex crystallography beamline (BL19U1) at the Shanghai Synchrotron Radiation Facility. Nucl Sci Tech 2019;30(11):170.
[22] Otwinowski Z, Minor W. Processing of X-ray diffraction data collected in oscillation mode. Methods Enzym 1997;276:307–26.
[23] Adams PD, Afonine PV, Bunkóczi G, Chen VB, Davis IW, Echols N, Headd JJ, Hung LW, Kapral GJ, Grosse-Kunstleve RW, McCoy AJ, Moriarty NW, Oeffner R, Read RJ, Richardson DC, Richardson JS, Terwilliger TC, Zwart PH. PHENIX: a comprehensive Python-based system for macromolecular structure solution. Acta Crystallogr D Biol Crystallogr 2010;66(2):213–21.
[24] Emsley P, Lohkamp B, Scott WG, Cowtan K. Features and development of Coot. Acta Crystallogr D Biol Crystallogr 2010;66(4):486–501.
[25] Vaguine AA, Richelle J, Wodak SJ. SFCHECK: a unified set of procedures for evaluating the quality of macromolecular structure-factor data and their agreement with the atomic model. Acta Crystallogr D Biol Crystallogr 1999;55(1):191–205.
[26] Pearlman DA, Case DA, Caldwell JW, Ross WS, Iii T, Debolt S, Ferguson D, Seibel G, Kollman P. AMBER, a package of computer programs for applying molecular mechanics, normal mode analysis, molecular dynamics and free energy calculations to simulate the structural and energetic properties of molecules. Comput Phys Commun 1995;91(1–3):1–41.
[27] Case DA, Cheatham TE, Darden T, Gohlke H, Luo R, Merz Jr KM, Onufriev A, Simmerling C, Wang B, Woods RJ. The Amber biomolecular simulation programs. J Comput Chem 2005;26(16):1668–88.
[28] Tian C, Kasavajhala K, Belfon KAA, Raguette L, Huang H, Migues AN, Bickel J, Wang Y, Pincay J, Wu Q, et al. ff19SB: amino-acid-specific protein backbone parameters trained against quantum mechanics energy surfaces in solution. J Chem Theory Comput 2020;16(1):528–52.
[29] Wang J, Wolf RM, Caldwell JW, Kollman PA, Case DA. Development and testing of a general amber force field. J Comput Chem 2004;25(9):1157–74.
[30] Pang YP. Successful molecular dynamics simulation of two zinc complexes bridged by a hydroxide in phosphotriesterase using the cationic dummy atom method. Proteins 2001;45(3):183–9.
[31] Izadi S, Anandakrishnan R, Onufriev AV. Building water models: a different approach. J Phys Chem Lett 2014;5(21):3863–71.
[32] Izadi S, Onufriev AV. Accuracy limit of rigid 3-point water models. J Chem Phys 2016;145(7):074501.
[33] Pastor RW, Brooks BR, Szabo A. An analysis of the accuracy of Langevin and molecular dynamics algorithms. Mol Phys 1988;65(6):1409–19.
[34] Feller SE, Zhang YH, Pastor RW, Brooks BR. Constant pressure molecular dynamics: the Langevin piston method. J Chem Phys 1994:103.
[35] Tr F, Smith W. SHAKE, rattle, and roll: efficient constraint algorithms for linked rigid bodies. J Comput Chem: Org, Inorg, Phys, Biol 2000;2:21.
[36] Darden T, York D, Pedersen L. Particle mesh Ewald: An Nlog(N) method for Ewald sums in large systems. J Chem Phys 1993;98(12):10089–92.
[37] Dai C, Feng P, Cui L, Su R, Chen W, Wei L. Iterative feature representation algorithm to improve the predictive performance of N7-methylguanosine sites. Brief Bioinform 2021;22:4.
[38] Zhang LS, Liu C, Ma H, Dai Q, Sun HL, Luo G, Zhang Z, Zhang L, Hu L, Dong X, et al. Transcriptome-wide mapping of internal N7-methylguanosine methylome in mammalian mRNA. Mol Cell 2019;74(6):1304–16. e1308.
[39] He C. Grand challenge commentary: RNA epigenetics? Nat Chem Biol 2010;6(12):863–5.
[40] Fang Z, Hu Y, Chen J, Xu K, Wang K, Zheng S, Guo C. Mass Spectrometry-based targeted serum monomethylated ribonucleosides profiling for early detection of breast cancer. Front Mol Biosci 2021;8:741603.
[41] Martínez L. Automatic identification of mobile and rigid substructures in molecular dynamics simulations and fractional structural fluctuation analysis. PLoS One 2015;10(3):e0119264.
[42] Kim TH, Mehrabi P, Ren Z, Sljoka A, Ing C, Bezginov A, Ye L, Pomès R, Prosser RS, Pai EF. The role of dimer asymmetry and protomer dynamics in enzyme catalysis. Science 2017;355:6322.
[43] Mehrabi P, Schulz EC, Dsouza R, Müller-Werkmeister HM, Tellkamp F, Miller RJD, Pai EF. Time-resolved crystallography reveals allosteric communication aligned with molecular breathing. Science 2019;365(6458):1167–70.
[44] Chen H, Wei P, Huang C, Tan L, Liu Y, Lai L. Only one protomer is active in the dimer of SARS 3C-like proteinase. J Biol Chem 2006;281(20):13894–8.
[45] Rangarajan ES, Izard T. Dimer asymmetry defines α-catenin interactions. Nat Struct Mol Biol 2013;20(2):188–93.